

Dual Nanoparticle Amplified SPR Detection of Thrombin at Subattomolar Concentrations

Seung Hee Baek^a, Alastair W. Wark^b and Hye Jin Lee^{a*}

^aDepartment of Chemistry and Green-Nano Materials Research Center, Kyungpook National University, 1370 Sankyuk-dong, Buk-gu, Daegu-city, 702-701, Republic of Korea

^bCentre for Molecular Nanometrology, WestCHEM, Department of Pure and Applied Chemistry, University of Strathclyde, Glasgow, UK, G1 1XL

****Corresponding author:** Tel. + 82 053 950 5336; Fax +82 053 950 6330; e-mail address: hyejinlee@knu.ac.kr; postal address: Department of Chemistry and Green-Nano Materials Research Center, Kyungpook National University, 1370 Sankyuk-dong, Buk-gu, Daegu-city, 702-701, Republic of Korea*

Abstract

A novel dual nanoparticle amplification approach is introduced for the enhanced surface plasmon resonance (SPR) detection of a target protein at subattomolar concentrations. Thrombin was used as a model target protein as part of a sandwich assay involving an anti-thrombin (anti-Th) modified SPR chip surface and a thrombin specific DNA aptamer (Th-aptamer) whose sequence also includes a polyadenine (A_{30}) tail. Dual nanoparticle (NP) enhancement was achieved with the controlled hybridization adsorption of first polythymine-NP conjugates (T_{20} -NPs) followed by polyadenine-NP's (A_{30} -NPs). Two different nanoparticle shapes (nanorod and quasi-spherical) were explored resulting in four different NP pair combinations being directly compared. It was found that both the order and NP shape were important in optimizing the assay performance. The use of real-time SPR measurements to detect target concentrations as low as 0.1 aM is a ten-fold improvement compared to single NP-enhanced SPR detection methods.

Introduction

Metallic nanoparticles with controlled size, shape and surface chemistry have enabled a wide range of new opportunities to be explored for performing very sensitive optical measurements of biomolecular interactions.¹⁻⁵ When combined with surface plasmon resonance (SPR) chip-based techniques as part of a sandwich assay format, detection limits ranging from the low picomolar to attomolar (aM) have been reported.⁶⁻¹⁴ In comparison, a typical SPR detection limit based on the specific adsorption of a target protein onto a planar gold film with no further signal amplification is ~1-10 nM.^{15,16} Most NP-enhanced SPR studies reported previously have focused on a single nanoparticle specific adsorption step.^{6-9,11-14} Alternative amplification strategies such as surface polymerization,^{13,17,18} metal deposition,¹⁹⁻²¹ enzyme-substrate turnover,²²⁻²⁵ can also be highly sensitive. However, achieving good control over both signal reproducibility and dynamic range in such multi-step amplification processes is challenging.

In this article, we demonstrate for the first time a controlled dual nanoparticle SPR amplification approach capable of detecting a target protein at subattomolar concentrations. The incorporation of two different gold nanoparticle shapes, nanorods (NRs) and quasi-spherical nanoparticles (qsNPs), into the enhancement methodology is explored with both having at least one dimension of ~50 nm. Recently, we have shown that both these particle types resulted in a greater signal enhancement compared to other shapes and smaller particle sizes.^{12,14,26} This was for a single NP amplification step and the aim here was to create a two-step amplification strategy and determine if this resulted in an improved sensing performance. The clustering of magnetic particles on an SPR chip surface has been previously reported for signal amplification.²⁷ Also, the development of sensing platforms based on nanoparticle pair

formation has been described as part of a lateral flow assay²⁸ and also directly measuring individual nanoparticle pairs and single particles.²⁹⁻³¹ However, an approach based on two separate NP amplification steps following a protein molecule bioaffinity adsorption step onto a SPR surface has not been previously described to our knowledge. To address this, we employed thrombin as a model target, which is a well-established biomarker for anti-coagulation.^{32,33} The main reason for this selection is our approach requires a sandwich assay where at least one of the affinity probes is a nucleic acid aptamer. Also, SPR sensing using an anti-thrombin and DNA aptamer pair has been previously demonstrated by us¹² and provides a starting point for developing the amplification approach described here. This involves appending a polyadenine tail to the aptamer probe sequence as a platform for the sequential hybridization adsorption of complementary DNA-NP conjugates. A number of parameters including the combination of NPs used and the order they were introduced to the SPR chip surface as well as NP concentration were considered to successfully optimize the dual NP sensor performance resulting in a ten-fold enhancement compared to that of a single NP amplification.

Experimental Section

Further details on the chemicals and protocols used beyond the key points covered below are provided in the Supporting Information.

DNA Functionalization of Au Nanoparticles: A detailed procedure can be found in the Supporting Information. The Au quasi-spherical and rod shaped nanoparticles were synthesized using the methods described by Murphy *et al.*³⁴ and Nikoobakht *et al.*³⁵ respectively. The nanoparticles were then stabilized with 11-mercaptopundecanoic acid

(MUA) followed by the covalent attachment of 5'-end amine modified DNA (i.e. T₂₀, A₂₀, A₃₀, C₂₀) via EDC/NHSS linking chemistry. Nanoparticles were characterized utilizing UV-vis spectroscopy and transmission electron microscopy (TEM) analysis. In addition, further UV-vis measurements were performed for monitoring the mixing of DNA-NPs with complementary or non-complementary DNA-NPs (see Figures 2, S3-6); the first nanoparticle colloid was coated with T₂₀ and the nanoparticles subsequently added were coated with A₃₀. For negative control measurements, C₂₀ functionalized particles were used instead of A₃₀. When two different nanoparticle shapes were mixed the relative ratio of extinction values at the LSPR λ_{max} for qsNP : NR was 1:2 and when the same nanoparticle shapes were mixed, a 1:1 ratio was used. Any resulting changes in the UV-vis spectra due to hybridization were recorded every 30 min.

Fabrication of Antibody Biochips for SPR Measurements: Bare gold chips for SPR were purchased from Biacore. Anti-thrombin was immobilized on a chemically modified gold surface using EDC/NHSS linking chemistry. Briefly, a mixed monolayer was formed by soaking bare gold chips in the mixed ethanolic solution of 60% 1 mM MUA and 40% 1 mM PEG-SH (MW = 1530, Paraon Ltd.) for 12 h followed by washing the chip with ethanol and DI water. The use of PEG was essential for reducing possible non-specific adsorption. Next, the chip was exposed to the mixture of 7.5 mM EDC and 1.5 mM sulfo-NHS solution for 30 min resulting in the formation of a carboxylic acid terminated surface. The chip was then rinsed thoroughly with DI water. 1 μ L of 1 μ M anti-thrombin was then dropped on to the chip and covered with a cover slip and placed in a humidity chamber for at least 3 h. The antibody chip was then rinsed with DI water and kept at room temperature prior to measurements. 20 mM N-(2-hydroxyethyl)piperazine-N-(2-ethanesulfonic acid) (HEPES, Sigma-Aldrich) buffer containing 150 mM NaCl, 2 mM CaCl₂ (pH 7.4) was used throughout the experiments.

A Biacore 3000 SPR system was used with a constant flow of 5 $\mu\text{L}/\text{min}$ for all experiments. This instrument has four different sample injection channels on each SPR chip with two of the channels utilized for thrombin detection and the remaining two channels used for control measurements. Also, for all SPR measurements in Figures 3-4 and S7-8, only NR batches were used which had a λ_{max} of 767(± 7) nm after DNA modification. Similarly, only qsNP's with a λ_{max} of 531(± 2) nm were utilized. For thrombin detection, the target was flowed over the antibody immobilized gold chip for a minimum of 1 h to reach a steady-state surface coverage. This procedure was repeated for all thrombin concentrations and control measurements. The concentration of Th-aptamer used for the formation of the sandwich assay was maintained at 100 nM for all experiments while the concentrations of the qsNP and NR DNA conjugates were fixed at 0.10 nM and 0.13 nM, respectively. Control adsorption measurements were simultaneously performed in the chip reference channels with the choice of negative controls listed in Table 1 depending upon each set of measurements. Details of additional supporting experiments involving dark-field imaging of nanoparticle adsorption on a functionalized gold chip surface are described in the Supporting Information along with further details on the materials and methods used.

Results and Discussion

Dual NP-enhanced Detection Methodology: An overview of the dual nanoparticle enhanced SPR detection method is outlined in Figure 1 along with the different combinations of nanoparticles that were investigated. The first key step involves creating a sandwich assay on an antibody modified SPR chip (see the central dotted box in Figure 1). Thrombin was chosen as a model target as it has two separate epitope sites enabling specific binding to an antibody (anti-thrombin) and a DNA aptamer (Th-aptamer) simultaneously. Also, this

enabled the advantages of the dual nanoparticle approach to be readily assessed by comparing to previous work by ourselves¹² for the same target. Following the specific binding of thrombin to anti-thrombin, the SPR chip surface is exposed to a modified Th-aptamer sequence also featuring a long A₃₀ tail at the 3' end. Amplification of the SPR response is then achieved through the specific hybridization adsorption of a T₂₀ DNA–NP conjugate followed by a second step involving the specific binding of an A₃₀ DNA functionalized nanoparticle.

Two different nanoparticles were employed in this study: qsNPs with an average diameter of 50(±5) nm, and NRs with an average aspect ratio of 5 (length 50(±10) nm, width 10(±2) nm). Representative TEM images are shown in the Supporting Information (Figure S1) and extinction measurements of both Au nanoparticle solutions before and after DNA conjugation are provided in Figures 2a-b and S2. The qsNPs have a LSPR λ_{max} value of 533(±3) nm compared to 767(±7) nm for the NR sample.

To achieve dual nanoparticle amplification, different combinations of both nanoparticle shapes were investigated resulting in the four distinct signal enhancement strategies highlighted in Figure 1. In each case (a)-(d), the first amplification step involves either a T₂₀ modified qsNP or NR interacting specifically with the surface bound A₃₀ tail of the Th-aptamer/Th/anti-thrombin complex. Dual amplification is then achieved by next exposing the SPR chip surface to a colloidal solution of either the same nanoparticle shape or the other with the particles instead modified with A₃₀. In addition to observing a shift in the LSPR λ_{max} upon DNA modification (see Figures 2a-b and S2), a series of UV-vis measurements were performed for each of the four nanoparticle combinations. Examples of these measurements

are shown in Figures 2c-d where the interaction between A₃₀-qsNPs and T₂₀-NRs and also between A₃₀-NRs and T₂₀-NRs are monitored, respectively. In both cases, a significant broadening and red-shift in the LSPR peaks occurs as expected for NP aggregate formation.^{5,36,37} Further nanoparticle combinations and controls are shown in the supporting information (Figures S3-6).

Subattomolar Thrombin Detection: The main focus of this study was to explore if a surface-based dual nanoparticle amplified SPR approach could be successfully applied for the detection of a non-modified thrombin target and quantify the resulting improvements in sensing performance. Figure 3 compares a series of detection and non-specific control (labeled NC) measurements for each of the four sensing configurations outlined previously in Figure 1. In each case, the anti-thrombin modified SPR chip was first exposed to a 0.1 aM solution of thrombin at a constant flow rate of 5 μ L/min for at least 1 h to ensure a steady-state surface coverage is reached due to the slow Langmuir adsorption kinetics at such low concentrations. A 100 nM solution of the secondary Th-aptamer probe is then flowed across the SPR chip for a fixed period of 20 min to form the surface-based anti-thrombin/Th/Th-aptamer complex. The Langmuir adsorption coefficient between thrombin and the Th-aptamer sequence has been previously measured by us¹² as $2.2(\pm 3) \times 10^7 \text{ M}^{-1}$ while an adsorption coefficient of about $10^7\text{--}10^8 \text{ M}^{-1}$ has been reported for the anti-thrombin interaction.^{38,39} At such a low target concentration, no detectable signal change occurs when the SPR chip was exposed to both the thrombin and 100 nM Th-aptamer solutions; however, upon injection of the first nanoparticle solution, a signal increase is observed due to a combination of both specific and non-specific nanoparticle adsorption as well as a temporary change in refractive index of the bulk solution. Following a brief HEPES buffer rinse for 15

min, the second nanoparticle solution is then introduced. For all measurements, the nanoparticle injection times were also fixed at 30 min. While this results in an overall analysis time of close to 3 h, prior sample modification or pre-concentration steps is not required to achieve very sensitive measurements.

The concentrations of the functionalized nanoparticles used to amplify the SPR detection signal were kept at the same values for all the measurements reported here. Based on UV-vis measurements, the extinction of the DNA-NPs conjugates was maintained at 0.5 for the NR-DNA conjugates and a value of 0.25 for the qsNP conjugates. Corresponding measurements using a Nanosight LM20 instrument were performed from which particle concentrations of the stock solutions were estimated. For the qsNPs, this corresponded to 0.10 nM with a calculated extinction coefficient of $2.4 \times 10^9 \text{ M}^{-1}$ at the LSPR λ_{max} while for the nanorod stock this was 0.13 nM with the measured extinction coefficient of $4.0 \times 10^9 \text{ M}^{-1}$ comparable with that expected from the literature.⁴⁰ Note that these nanoparticle concentrations are slightly lower than those used in our previous work¹² which focused on optimizing the enhancement from a single nanoparticle amplification step. This was necessary as the use of higher NP concentrations resulted in the unsuccessful implementation of the dual amplification due to saturation of the SPR response. Also, in all experiments, a fixed nanoparticle injection time of 30 min was consistently applied for simplicity even though the SPR signal did not reach a steady-state value for every measurement.

The basis for demonstrating dual nanoparticle amplification is to show a greater SPR signal enhancement for the specific adsorption of complementary DNA functionalized nanoparticles across both the first and second NP binding steps compared to non-complementary control

measurements. Comparison of the data sets in Figure 3 show that the data curves for 0.1 aM detection are all consistently higher for the various NC curves (which are discussed in more detail further below). For the first nanoparticle amplification step the signal change is higher for the qsNPs than for the NRs when analyzed alongside the corresponding NC data curves. This observation agrees with our previous study where a greater signal enhancement for the qsNPs was associated with the larger volume particle, which results in a larger refractive change at the SPR chip surface compared to the smaller NR's for the same number of surface binding events.¹² It is also the main reason why the NR concentration described above was higher than that of the qsNP conjugates. More interestingly, the amplification strength of the second nanoparticle surface binding step differs from the trends observed for the first stage. In Figure 3a, the signal amplification associated with the secondary qsNP surface binding step is 10.8 times greater than that of the first NR amplification. On reversing the qsNP and NR order (Figure 3b), a much smaller enhancement in signal was observed due to the second NR adsorption step. However, when two NRs are utilized (Figure 3c), the second NR adsorption step results in an amplified SPR response 3.8 times greater than that associated with the first NR measurement. Overall, the largest combined enhancement across both nanoparticle steps is for the qsNP pair shown in Figure 3d, where the signal amplification was approximately similar for both steps. However, the largest second step amplification is observed for the T₂₀-NR / A₃₀-qsNP combination.

Figure 4 displays the results for a series of measurements acquired at different thrombin concentrations using the T₂₀-NR / A₃₀-qsNP dual amplification. The normalized change in SPR signals shown in Figure 4b were calculated by subtracting the highest of the NC control values from the thrombin detection channel signal. A linear response range was obtained over

a relatively narrow concentration range (0.1 to 2 aM), above which further increases in signal were considerably smaller. This small dynamic range is typical of SPR measurements involving large signal amplification strategies and different protein concentrations can be targeted depending on the nanoparticle bulk concentration.¹⁴ Attempts to measure thrombin concentrations below 0.1 aM were unsuccessful, however this is still a significant ten-fold improvement on previous measurements involving a single nanoparticle amplification step.¹²

An entire repeat set of the measurements described in Figures 3 and 4 including controls are shown in the supporting information (Figures S7 and 8) where the only difference is that the polyadenine sequence used in the second nanoparticle amplification step is 20 bases long instead of 30. The same data trends described in Figures 3 and 4 were observed again with no significant difference in the detection performance. In general, when a NR is used in the first amplification step, a much higher signal increase is observed for the second step for both qsNP's and NR's. On the other hand, when qsNPs are used in the first amplification step, a secondary nanorod step results in little further enhancement. These observations raise a question on whether it is a relative difference in binding affinity between the nanoparticle conjugates (due to shape and DNA surface coverage) or if there are stronger SPR and LSPR plasmonic coupling effects depending on the NP binding order. The qsNP's consistently result in a higher enhancement compared to the NR's for a single binding event in either the first or second steps. Also, the NR SPR data curves do not always reach a steady-state surface coverage over the same injection timescale, which suggests a lower DNA surface coverage than for the qsNP's. However, attempting to disentangle the LSPR and physical NP contributions to the overall enhancement requires a further detailed study at the single nanoparticle level. While there has been work demonstrating the plasmon shifts associated

with single metallic particles on gold films⁴¹ and also experimental and theoretical studies of nanoparticle pairs,⁴²⁻⁴⁴ a spectral investigation of individual NP pairs comparing both in the presence and absence of a gold film has yet to be performed that we are aware of and an investigation is now underway.

Non-specific Adsorption: One of the main challenges of performing measurements at extremely low target concentrations is the issue of non-specific adsorption of nanoparticles onto the SPR chip surface. Consequently, all of the SPR measurements described above were supported by a number of non-specific controls (NC1 to NC16) covering all four dual nanoparticle combinations, with each described in Table 1. These were designed to enable a direct comparison of specific and non-specific interactions for both nanoparticle types at each of the first and second amplification steps. For example, NC1-4 applies to the NR (first) / qsNP (second) combination where, for NC1 to 3, the initial anti-thrombin/Th/Th-aptamer surface complex is formed under identical conditions to that within the detection channel. For NC4, the same combination of nanoparticle-DNA conjugates is used as for the actual measurement except no target or aptamer was introduced to the SPR chip surface. The same pattern of controls was also applied for the remaining three NR and qsNP dual combinations.

Representative control curves obtained from the SPR chip reference channels during repeat runs are presented in each of the data series in Figures 3 and S7. The most likely explanation for non-specific behavior is electrostatic interactions between the nanoparticle and SPR chip. Across all the control measurements listed in Table 1, it is possible to compare the overall change in SPR signal over both amplification stages as well as compare relative changes between the two amplification steps and nanoparticle types. Firstly, increases in background

signal following rinsing with buffer can be clearly seen for all NC measurements indicating some degree of non-specific adsorption. In terms of the absolute change in the SPR response, both the positive and control signals are generally lower for the NR's than the qsNP's. When comparing relative differences between the positive and NC data curves, some general comments can be made. If the 1st amplification step involves a nonmatching NP (e.g. NC 2, 14) then the background signal is lower for both NP types than when the 1st NP matches that of the positive data (e.g. NC 7, 15). In addition, the control signal tends to be lowest when no target or aptamer is introduced to the reference channel (e.g. NC 8, 12). There are exceptions to these generalizations due to variability of the non-specific adsorption, hence why all data measurements were compared with the highest non-specific response among the controls. However, it is clear from the acquired data that the ratio of specific to non-specific signal is consistently higher for the qsNP's than for the NR's.

To gain some further insight and provide direct evidence of specific and non-specific nanoparticle adsorption behavior, a series of *in-situ* dark-field imaging measurements were performed. This is described in the supporting information where images were acquired of particle adsorption on the same chip area before and after each amplification step for both the NR / qsNP (Figure S9) and the NR / NR (Figure S10) dual amplification combinations. A set of control measurements is also shown in each figure. The experimental conditions were kept the same as for the SPR measurements except a different Au chip with a thin glass cell window enabling *in-situ* imaging is used. In both sets of measurements, a number of scattering features can be observed in the optical path before exposure of the surface to DNA-nanoparticle conjugates. Following the first nanoparticle adsorption step, the presence of adsorbed particles can be easily detected. For the NR / NR combination, no significant

changes in particle density are discernible between the first and second amplification steps with the surface coverage double that of the control measurement. For the NR / qSNP combination, an increase in particle density is observed after each step for both sample and control with the differences in surface coverage less than ~8%. These preliminary measurements highlight the importance of non-specific controls and further efforts are underway to combine SPR and *in-situ* dark-field imaging to improve detection performance at very low target concentrations. It is also worth pointing out that the surface area probed in a single channel on the SPR chip is $\sim 36 \times$ greater than the field of view in the dark-field measurements which will enable greater discrimination in changes in particle surface coverage compared to the microscope field of view.

Conclusions

In this article, we have successfully demonstrated a new strategy for the enhanced SPR detection of protein bioaffinity interactions based on the controlled sequential adsorption of two different NP-DNA conjugates onto a chip surface. This was achieved through the use of a sandwich assay involving a nucleic acid aptamer whose sequence can be easily modified with an extended polyadenine tail to provide a binding site for specific NP adsorption. A significant advantage of the use of aptamers compared to antibody probes is that this approach can be readily adapted to any aptamer/antibody or aptamer/aptamer sandwich assay combination with the number of examples of both continuing to rise in the literature.⁴⁵⁻⁴⁸ Furthermore, by exploring different nanoparticle shapes we highlight the versatility of this approach and we also expect the use of different modified DNA sequences binding to the aptamer will expand this approach to other surface-based signal transduction mechanisms such as electrochemistry.⁴⁹ As well as developing a new amplification mechanism, it was

demonstrated that even further improvements in sensitivity could be achieved compared to previous efforts focusing on a single nanoparticle amplification step. For measurements at higher concentrations than the very low $\sim 0.1 - 4$ aM range used here, it is likely that a single NP amplification strategy will be sufficient, especially if a larger NP size such as the ~ 50 nm qSNP's used here is employed. However, the issue of non-specific adsorption of nanoparticles on sensor surfaces remains a significant challenge as highlighted by the dark-field measurements here. As the field of nanoparticle enhanced sensing continues to evolve with systematic studies of different nanoparticle types and surface chemistries we believe that the dual amplification strategy outlined here will be a valuable route towards more sensitive surface bioaffinity measurements.

Acknowledgement

This research was supported by both Basic Science Research Program through the National Research Foundation of Korea (NRF) funded by the Ministry of Science, ICT and Future Planning (NRF-2013R1A2A2A03068833).

Supporting Information

Further experimental details include materials used, synthesis of nanoparticles and their biofunctionalization as well as fabrication of antibody biochips for SPR and dark-field imaging measurements. Figures S1-10 include TEM, UV-Vis, SPR and dark-field imaging data. This information is available free of charge via the Internet at <http://pubs.acs.org>.

References

- (1) Fritzsche, W.; Taton, T. A. *Nanotechnology* **2003**, *14*, R63-73.
- (2) Wang, J. *Small* **2005**, *1*, 1036-1043.
- (3) Cao, X.; Ye, Y.; Liu, S. *Anal. Biochem.* **2011**, *417*, 1-16.
- (4) Perfézou, M.; Turner, A.; Merkoçi, A. *Chem. Soc. Rev.* **2012**, *41*, 2606-2622.
- (5) Fong, K. E.; Yung, L.-Y. L. *Nanoscale* **2013**, *5*, 12043-12071.
- (6) He, L.; Musick, M. D.; Nicewarner, S. R.; Salinas, F. G.; Benkovic, S. J.; Natan, M. J.; Keating, C. D. *J. Am. Chem. Soc.* **2000**, *122*, 9071-9077.
- (7) Hayashida, M.; Yamaguchi, A.; Misawa, H. *Jpn. J. Appl. Phys.* **2005**, *44*, L1544-1546.
- (8) Lee, H. J.; Wark, A. W.; Corn, R. M. *Analyst*, **2008**, *133*, 596-601.
- (9) Wang, J.; Munir, A.; Li, Z.; Zhou, H. S. *Biosens. Bioelectron.* **2009**, *25*, 124-129.
- (10) D'Agata, R.; Corradini, R.; Ferretti, C.; Zanolli, L.; Gatti, M.; Marchelli, R.; Spoto, G. *Biosens. Bioelectron.* **2010**, *25*, 2095-2100.
- (11) Sendroiu, I. E.; Gifford, L. K.; Lupták, A.; Corn, R. M. *J. Am. Chem. Soc.* **2011**, *133*, 4271-4273.
- (12) Kwon, M. J.; Lee, J.; Wark, A. W.; Lee, H. J. *Anal. Chem.* **2012**, *84*, 1702-1707.
- (13) Liu, Y.; Cheng, Q. *Anal. Chem.* **2012**, *84*, 3179-3186.
- (14) Jang, H. R.; Wark, A. W.; Baek, S. H.; Chung, B. H.; Lee, H. J. *Anal. Chem.* **2014**, *86*, 814-819.
- (15) Stevens, R. C.; Soelberg, S. D.; Near, S.; Furlong, C. E. *Anal. Chem.* **2008**, *80*, 6747-6751.
- (16) Bolduc, O. R.; Pelletier, J. N.; Masson, J.-F. *Anal. Chem.* **2010**, *82*, 3699-3706.
- (17) Kim, Y.-R.; Paik, H.-J.; Ober, C. K.; Coates, G. W.; Mark, S. S.; Ryan, T. E.; Batt, C. A. *Macromol. Biosci.* **2006**, *6*, 145-152.
- (18) Liu, Y.; Dong, Y.; Jauw, J.; Linman, M. J.; Cheng, Q. *Anal. Chem.* **2010**, *82*, 3679-3685.
- (19) Taton, T. A.; Mirkin, C. A.; Letsinger, R. L. *Science* **2000**, *289*, 1757-1760.
- (20) Pavlov, V.; Xiao, Y.; Shlyahovsky, B.; Willner, I. *J. Am. Chem. Soc.* **2004**, *126*, 11768-11769.
- (21) Wang, Q.; Yang, X.; Wang, K. *Sens. Actuators, B* **2007**, *123*, 227-232.
- (22) Iwasaki, Y.; Horiuchi, T.; Niwa, O. *Anal. Chem.* **2001**, *73*, 1595-1598.
- (23) Lee, H. J.; Li, Y.; Wark, A. W.; Corn, R. M. *Anal. Chem.* **2005**, *77*, 5096-5100.
- (24) Xu, F.; Zhen, G.; Yu, F.; Kuennemann, E.; Textor, M.; Knoll, W. *J. Am. Chem. Soc.* **2005**, *127*, 13084-13085.
- (25) Li, Y.; Lee, H. J.; Corn, R. M. *Anal. Chem.* **2007**, *79*, 1082-1088.
- (26) Kim, S.; Lee, J.; Lee, S. J.; Lee, H. J. *Talanta* **2010**, *81*, 1755-1759.
- (27) Krishnan, S.; Mani, V.; Wasalathanthri, D.; Kumar, C. V.; Rusling, J. F. *Angew. Chem. Int. Ed.* **2011**, *50*, 1175-1178.
- (28) Choi, D. H.; Lee, S. K.; Oh, Y. K.; Bae, B. W.; Lee, S. D.; Kim, S.; Shin, Y.-B.; Kim, M.-G. *Biosens. Bioelectron.* **2010**, *25*, 1999-2002.
- (29) Chen, J. I. L.; Chen, Y.; Ginger, D. S. *J. Am. Chem. Soc.* **2010**, *132*, 9600-9601.
- (30) Ungureanu, F.; Wasserberg, D.; Yang, N.; Verdoold, R.; Kooyman, R. P. H. *Sens. Actuators, B* **2010**, *150*, 529-536.
- (31) Verdoold, R.; Gill, R.; Ungureanu, F.; Molenaar, R.; Kooyman, R. P. H. *Biosens. Bioelectron.* **2011**, *27*, 77-81.

- (32) Barnes, D. M.; Wakefield, T. W.; Rectenwald, J. E. *Biomarker Insights* **2008**, *3*, 93-100.
- (33) Hu, J.; Zheng, P.-C.; Jiang, J.-H.; Shen, G.-L.; Yu, R.-Q.; Liu, G.-K. *Anal. Chem.* **2009**, *81*, 87-93.
- (34) Sau, T. K.; Murphy, C. J. *J. Am. Chem. Soc.* **2004**, *126*, 8648-8649.
- (35) Nikoobakht, B.; El-Sayed, M. A. *Chem. Mater.* **2003**, *15*, 1957-1962.
- (36) Tabor, C.; Murali, R.; Mahmoud, M.; El-Sayed, M. A. *J. Phys. Chem. A* **2009**, *113*, 1946-1953.
- (37) Wang, Y.; Lee, K.; Irudayaraj, J. *Chem. Commun.* **2010**, *46*, 613-615.
- (38) Baerga-Ortiz, A.; Bergqvist, S.; Mandell, J. G.; Komives, E. A. *Protein Sci.* **2004**, *13*, 166-176.
- (39) Schlecht, U.; Malavé, A.; Gronewold, T.; Tewes, M.; Löhndorf, M. *Anal. Chim. Acta* **2006**, *573-574*, 65-68.
- (40) Orendorff, C. J.; Murphy, C. J. *J. Phys. Chem. B* **2006**, *110*, 3990-3994.
- (41) Hu, M.; Ghoshal, A.; Marquez, M.; Kik, P. G. *J. Phys. Chem. C* **2010**, *114*, 7509-7514.
- (42) Romero, I.; Aizpurua, J.; Bryant, G. W.; Abajo, F. J. G. *Optics Express* **2006**, *14*, 9988-9999.
- (43) Jain, P. K.; El-Sayed M. A. *Nano Lett.* **2008**, *8*, 4347-4352.
- (44) Dridi, M.; Vial, A. *Plasmonics* **2011**, *6*, 637-641.
- (45) O'Sullivan, C. K. *Anal. Bioanal. Chem.* **2002**, *372*, 44-48.
- (46) Song, S.; Wang, L.; Li, J.; Zhao, J.; Fan, C. *Trends in Anal. Chem.* **2008**, *27*, 108-117.
- (47) Lee, S. J.; Kwon, Y. S.; Lee, J.-E.; Choi, E.-J.; Lee, C.-H.; Song, J.-Y.; Gu, M. B. *Anal. Chem.* **2013**, *85*, 66-74.
- (48) Sabherwal, P.; Shorie, M.; Pathania, P.; Chaudhary, S.; Bhasin, K. K.; Bhalla, V., Suri, C. R. *Anal. Chem.* **2014**, 10.1021/ac501388a.
- (49) Nam, E. J.; Kim, E. J.; Wark, A. W.; Rho, S.; Kim, H.; Lee, H. J. *Analyst* **2012**, *137*, 2011-2016.

Figures

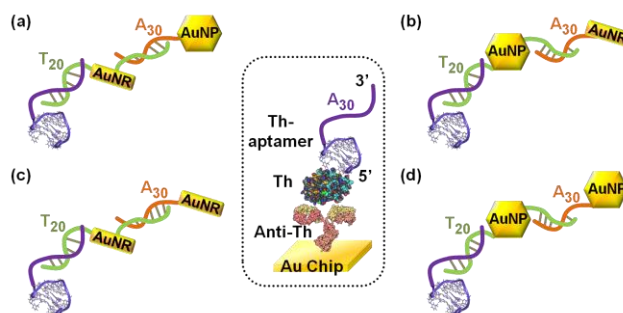


Figure 1. Schematic outlining different combinations of the dual nanoparticle enhanced SPR strategy for thrombin detection. The dotted box exhibits the formation of a surface sandwich complex of Th-aptamer/Th/anti-thrombin via the specific adsorption of the A₃₀ tailed thrombin aptamer followed by the adsorption of thrombin onto the surface tethered anti-thrombin. In (a)-(d), different approaches are described where a T₂₀ modified nanoparticle (qsNP or NR) binds specifically to the surface Th-aptamer followed by the hybridization adsorption of A₃₀ modified qsNPs or NRs, resulting in four different possible dual combinations.

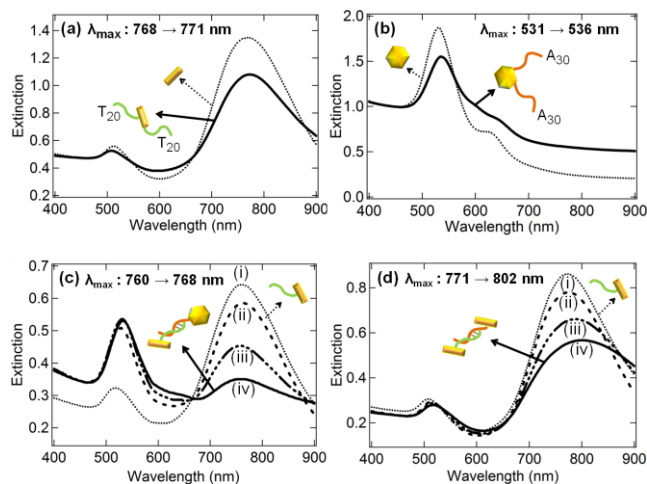


Figure 2. Representative extinction spectra of gold NRs (a) and qSNPs (b) comparing before (dotted line) and after (solid line) functionalization with T₂₀ and A₃₀ respectively. Extinction spectra monitoring both (c) T₂₀-NR / A₃₀-qSNP, and (d) T₂₀-NR / A₃₀-NR self-assembly due to DNA hybridization. In each case, curve (i) represents the starting NR conjugate solution before the addition of an equal volume of the second nanoparticle solution. (ii)-(iv) spectra were obtained at times of 10 sec, 30 min and 2 h, respectively, following mixing. Different batches of nanorods were used in these experiments which explains the ~15 nm variability in the starting LSPR.

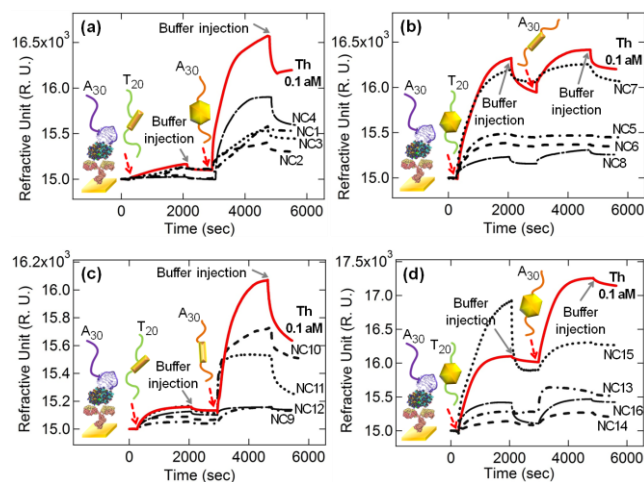


Figure 3. A series of SPR sensorgrams comparing four different nanoparticle pair combinations for the amplified detection of thrombin. Each measurement shown as a red line in (a) through (d) corresponds to the detection scheme indicated previously in Figures 1a-d. The thrombin target concentration was fixed at 0.1 aM for each measurement. The control measurements (NC1–NC16) are represented by the black data curves and correspond to the configurations summarized in Table 1.

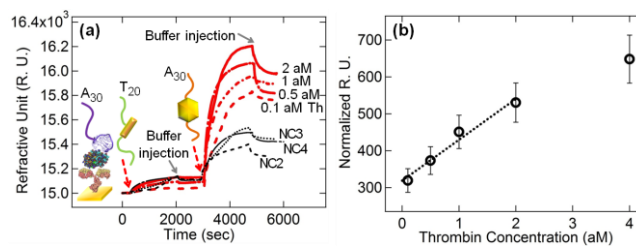

































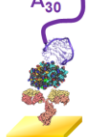
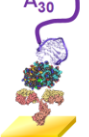
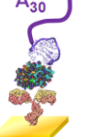



Figure 4. (a) Representative SPR sensorgrams for the dual T₂₀-NR / A₃₀-qsNP amplified detection of thrombin at various thrombin concentrations from 0.1 aM to 2 aM. (b) Plot showing linear SPR response range (dotted line) within thrombin concentrations measured from 0.1 aM to 4 aM with the normalized values calculated by taking the detection channel signal response and subtracting the highest NC signal. Error bars were calculated from an average of three repeat measurements.

Table 1. Schematic summary of negative controls used for investigating the non-specific adsorption of nanoparticles during the dual nanoparticle amplified SPR detection of thrombin. The columns labelled (a), (b), (c) and (d) correspond to the positive data curves in Figures 3 and S7. Note that A₂₀ coated NPs were used instead of A₃₀-NPs in Figure S7.

Number	(a)	NC1	NC2	NC3	NC4	(b)	NC5	NC6	NC7	NC8	(c)	NC9	NC10	NC11	NC12	(d)	NC13	NC14	NC15	NC16
2 nd NP	 A ₃₀	 T ₂₀	 A ₃₀	 T ₂₀	 A ₃₀	 A ₃₀	 T ₂₀	 A ₃₀	 T ₂₀	 A ₃₀	 A ₃₀	 T ₂₀	 A ₃₀	 T ₂₀	 A ₃₀	 A ₃₀	 T ₂₀	 A ₃₀	 T ₂₀	 A ₃₀
1 st NP	 T ₂₀	 A ₃₀		 T ₂₀		 T ₂₀	 A ₃₀		 T ₂₀		 T ₂₀	 A ₃₀		 T ₂₀		 T ₂₀	 A ₃₀		 T ₂₀	
Chip Surface																				

For TOC only

